

The CD38⁻CD20⁺ cells generated in our culture system have all the features of memory B cells: phenotype, ability to respond to proliferative signals, and low levels of intracytoplasmic and secreted Ig. Although most memory B cells isolated from human tonsils are medium-size resting B cells (7), the memory B cells generated here are large cells. Large memory B blasts have been identified in vivo in the B cell follicles, where they have been construed as long-term memory B cells undergoing chronic stimulation by immune complexes on follicular dendritic cells (1), and among the recirculating thoracic duct lymphocytes, where they have been construed as memory B cells recently generated from GCs (15). The generation of CD38⁻CD20⁺ memory B blasts from GC B cells described here will provide a model to identify the signals that allow such blasts to revert to small resting cells.

Our results show that interruption of the CD40 signal after 3 days of primary culture results in the terminal differentiation of proliferating B blasts into plasma cells. They are characterized by typical phenotype and morphology, large amounts of intracellular Ig and secretion of large amounts of Ig, and the inability to undergo further proliferation. During humoral immune responses, responding B cells differentiate into either memory B cells or plasma cells. These two facets of the response must be tightly integrated to ensure adequate amounts of antibody production and the generation of memory B cells. CD40L plays a critical role at two stages of memory B cell generation: (i) in the induction phase of GC reaction, as demonstrated by the lack of GCs in hyper-IgM patients (16) and in mouse models where CD40-CD40L interactions were interrupted (17, 18), and (ii) in the differentiation phase of high-affinity GC B cells toward memory B cells, as demonstrated here. This second phase (CD40L-dependent GC B cell differentiation) was also suggested by an interesting in vivo observation: Mice receiving soluble CD40-IgG chimeric molecules have normal GCs but no memory B cell generation. Because soluble CD40-IgG chimeric molecules have a lower affinity for CD40L than do antibodies to CD40L, this observation suggests that the GC differentiation phase is more easily blocked than the GC induction phase (19). The recent identification of T cells that express CD40L in the light zone of GCs from human tonsils (9) supports the hypothesis that the GC differentiation phase occurs here (20). After somatic mutation and positive selection, high-affinity GC B cells pick up antigen from follicular dendritic cells and present it to GC T cells (20). During this cognate T-B cell interaction, T cells may be induced to secrete cytokines and to express CD40L (21), resulting in the

generation of CD38⁻CD20⁺ memory B blasts. Because CD40L expression on T cells can be rapidly down-regulated by CD40 antigen on B cells (11), a proportion of proliferating B blasts will differentiate into CD38⁺CD20⁻ plasma cells in the absence of CD40L signaling.

REFERENCES AND NOTES

1. Y.-J. Liu, J. Zhang, P. J. L. Lane, E. Y.-T. Chan, I. C. M. MacLennan, *Eur. J. Immunol.* **21**, 2951 (1991); J. Jacob and G. Kelsoe, *J. Exp. Med.* **176**, 679 (1992).
2. C. Berek, A. Berger, M. Apel, *Cell* **67**, 1121 (1991); J. Jacob, G. Kelsoe, K. Rajewsky, U. Weiss, *Nature* **354**, 389 (1991); R. Küppers, M. Zhao, M.-L. Hansmann, K. Rajewsky, *EMBO J.* **12**, 4955 (1993); M. G. MacHeyzer-Williams, M. J. MacLean, P. A. Lalor, G. J. V. Nossal, *J. Exp. Med.* **178**, 295 (1993).
3. R. F. Coico, B. S. Bhogal, G. J. Thorbecke, *J. Immunol.* **131**, 2254 (1983); G. B. Klaus, J. H. Humphrey, A. Kunkl, D. W. Dongworth, *Immunol. Rev.* **53**, 3 (1980).
4. M. H. Kosco, G. F. Burton, Z. F. Kapasi, A. K. Szakal, J. G. Tew, *Immunology* **68**, 312 (1989).
5. Y.-J. Liu *et al.*, *Nature* **342**, 929 (1989).
6. Y.-J. Liu and J. Banachereau, in *Handbook of Experimental Immunology*, L. A. Herzenberg, Ed. (Blackwell Scientific, Oxford, ed. 5, in press), vol. 2.
7. V. Pascual *et al.*, *J. Exp. Med.* **180**, 329 (1994).
8. H. Harada *et al.*, *Blood* **81**, 2658 (1993).
9. S. Lederman *et al.*, *J. Immunol.* **149**, 3817 (1992); M. Casamajor-Palleja, M. Kahn, I. C. M. MacLennan, *J. Exp. Med.*, in press.
10. A.-C. Flückiger, P. Garrone, I. Durand, J.-P. Galizzi, J. Banachereau, *J. Exp. Med.* **178**, 1473 (1993).
11. C. Van Kooten *et al.*, *Eur. J. Immunol.* **24**, 787 (1994).
12. A. Rolink, A. Kudo, H. Karasuyama, Y. Kikuchi, F.

- Melchers, *EMBO J.* **10**, 327 (1991).
13. E. A. Clark and J. A. Ledbetter, *Nature* **367**, 425 (1994); J. Banachereau and F. Rousset, *ibid.* **353**, 678 (1991).
14. M. J. Holder *et al.*, *Int. Immunol.* **5**, 1059 (1993).
15. S. Strober, *J. Immunol.* **117**, 1288 (1976).
16. U. Korthäuer *et al.*, *Nature* **361**, 539 (1993).
17. T. Kawabe *et al.*, *Immunity* **1**, 167 (1994); J. Xu *et al.*, *ibid.*, p. 423.
18. T. M. Foy *et al.*, *J. Exp. Med.* **180**, 157 (1994).
19. D. Gray, P. Dullforce, S. Jainandunsing, *ibid.*, p. 141.
20. Y.-J. Liu, G. D. Johnson, J. Gordon, I. C. M. MacLennan, *Immunol. Today* **13**, 17 (1992); I. C. M. MacLennan, *Annu. Rev. Immunol.* **12**, 117 (1994); G. J. Thorbecke, A. R. Amin, V. K. Tsiagbe, *FASEB J.* **8**, 832 (1994).
21. A. W. Butch, G.-H. Chung, J. W. Hoffmann, M. H. Nahm, *J. Immunol.* **150**, 39 (1993); J. Andersson *et al.*, *Immunology* **83**, 16 (1994).
22. Y.-J. Liu *et al.*, *Immunity*, in press.
23. GC B cells were isolated from total tonsillar B cells as described (6, 22). The purity of isolated GC B cells (Fig. 1A) was greater than 98% in all experiments. Their GC nature was confirmed by their mutated immunoglobulin V genes (7). For the primary culture, cells (10⁶/ml) were cultured with IL-10 (100 ng/ml) and IL-2 (10 U/ml) on CD40L-transfected murine fibroblasts (2 × 10⁵ fibroblasts per milliliter) irradiated with 75 Gy (where 1 Gy equals 100 rads) in Iscove medium containing 5% fetal calf serum for 3 days (10). For the secondary culture, the cells were washed and recultured for 4 days under three conditions, as described in the text. The antibody to CD40L used in the third condition was LL2 (C. Van Kooten, in preparation).
24. We thank I. Durand for FACS sorting, N. Courbière and M. Vatan for editorial help, I. C. M. MacLennan for communicating the manuscript in press, and J. Chiller for support. C.A., J.D., P.M., and G.G. received fellowships from the Fondation Mérieux.

30 November 1994; accepted 6 February 1995

Immune System Impairment and Hepatic Fibrosis in Mice Lacking the Dioxin-Binding Ah Receptor

Pedro Fernandez-Salguero, Thierry Pineau, David M. Hilbert, Timothy McPhail, Susanna S. T. Lee, Shioko Kimura, Daniel W. Nebert, Stuart Rudikoff, Jerrold M. Ward, Frank J. Gonzalez*

The aryl hydrocarbon (Ah) receptor (AHR) mediates many carcinogenic and teratogenic effects of environmentally toxic chemicals such as dioxin. An AHR-deficient (*Ahr*^{-/-}) mouse line was constructed by homologous recombination in embryonic stem cells. Almost half of the mice died shortly after birth, whereas survivors reached maturity and were fertile. The *Ahr*^{-/-} mice showed decreased accumulation of lymphocytes in the spleen and lymph nodes, but not in the thymus. The livers of *Ahr*^{-/-} mice were reduced in size by 50 percent and showed bile duct fibrosis. *Ahr*^{-/-} mice were also nonresponsive with regard to dioxin-mediated induction of genes encoding enzymes that catalyze the metabolism of foreign compounds. Thus, the AHR plays an important role in the development of the liver and the immune system.

The AHR is a ligand-activated transcription factor that is distinct from members of the steroid receptor superfamily (1). It is a member of the basic helix-loop-helix (bHLH) superfamily of DNA binding proteins and is activated by ligand binding and by dimerization with the AHR nuclear trans-

locator (Arnt) (1, 2). A functional AHR is required in laboratory animals to mediate the harmful effects of toxic environmental chemicals such as dioxin (2,3,7,8-tetrachlorodibenzo-*p*-dioxin, or TCDD), benzo[*a*]pyrene in cigarette smoke and the products of other combustion processes, poly-

chlorinated biphenyls, and polybrominated biphenyls (3–7). The AHR is constitutively expressed in many mammalian tissues, with the highest amounts of mRNA in liver, kidney, lung, heart, thymus, and placenta (8, 9). Dioxin-inducible genes regulated by the AHR include those encoding cytochromes P450 (*Cyp1a1*, *Cyp1a2*, and *Cyp1b1*) (10–12), phase II enzymes such as uridine diphosphate (UDP)–glucuronosyltransferase1*06 (*Ugt1*06*), and other growth factors and proteins (6, 13).

An endogenous ligand for the AHR has been postulated to play a critical role in

embryonic development and homeostasis (14). In addition, a role for the AHR in dioxin-mediated teratogenesis, apoptosis, immunosuppression, and cell type-specific proliferation (4–7) would support the view that this transcription factor regulates critical life functions. We now describe the construction and characterization of an AHR-deficient mouse line. Our results suggest that the AHR is important in the expression of dioxin-inducible genes and in normal development of the liver and the immune system.

The *Ahr* gene was inactivated in J1 embryonic stem (ES) cells by homologous recombination (15) with the use of a positive-negative selection strategy (16). A 7.5-kb fragment from a 129/SV mouse genomic clone containing exon 1 of *Ahr* was isolated, mapped, and partially sequenced (Fig. 1A). Exon 1, which encodes most of the basic region that participates in DNA binding, was replaced with a neomycin-resistance cassette that contained the bacterial phosphoribosyltransferase II gene (*neo*) as a positive selection marker. This construct was ligated to a thymidine kinase cassette

(as a negative selection marker) under the control of the herpes simplex virus promoter (HSV-TK). The construct was linearized and introduced into ES cells by electroporation. Of 980 clones screened, 3 represented a legitimate homologous recombination event and were injected into 3.5-day-old C57BL/6N mouse embryos. All the chimeras obtained showed a large 129/SV contribution, as judged from coat color. The male chimeras were mated with C57BL/6N females to give rise to heterozygotes, which were then interbred to produce an *Ahr* homozygous mutant colony. We screened mice for the presence of the targeted allele by Southern blot analysis of tail genomic DNA (Fig. 1B).

Of 260 animals screened from heterozygous matings, the relative frequencies of wild-type (*Ahr*^{+/+}), heterozygous (*Ahr*^{+/-}), and homozygous mutant (*Ahr*^{-/-}) mice at birth were 1:2:1, in accordance with normal Mendelian distribution and indicating no lethality during in utero development. Between 40 and 50% of the homozygous mutant (*Ahr*^{-/-}) mice died or were selectively cannibalized within 1 to 4 days after

P. Fernandez-Salguero, T. Pineau, S. S. T. Lee, S. Kimura, F. J. Gonzalez, Laboratory of Molecular Carcinogenesis, National Cancer Institute (NCI), National Institutes of Health (NIH), Bethesda, MD 20892, USA.
 D. M. Hilbert and S. Rudikoff, Laboratory of Genetics, NCI, NIH, Bethesda, MD 20892, USA.
 T. McPhail, Unit on Molecular Genetics, National Institute of Mental Health, NIH, Bethesda, MD 20892, USA.
 D. W. Nebert, Department of Environmental Health, University of Cincinnati Medical Center, Cincinnati, OH 45267, USA.
 J. M. Ward, Veterinary and Tumor Pathology Section, Office of Laboratory Animal Science, NCI, Frederick, MD 21702, USA.

*To whom correspondence should be addressed.

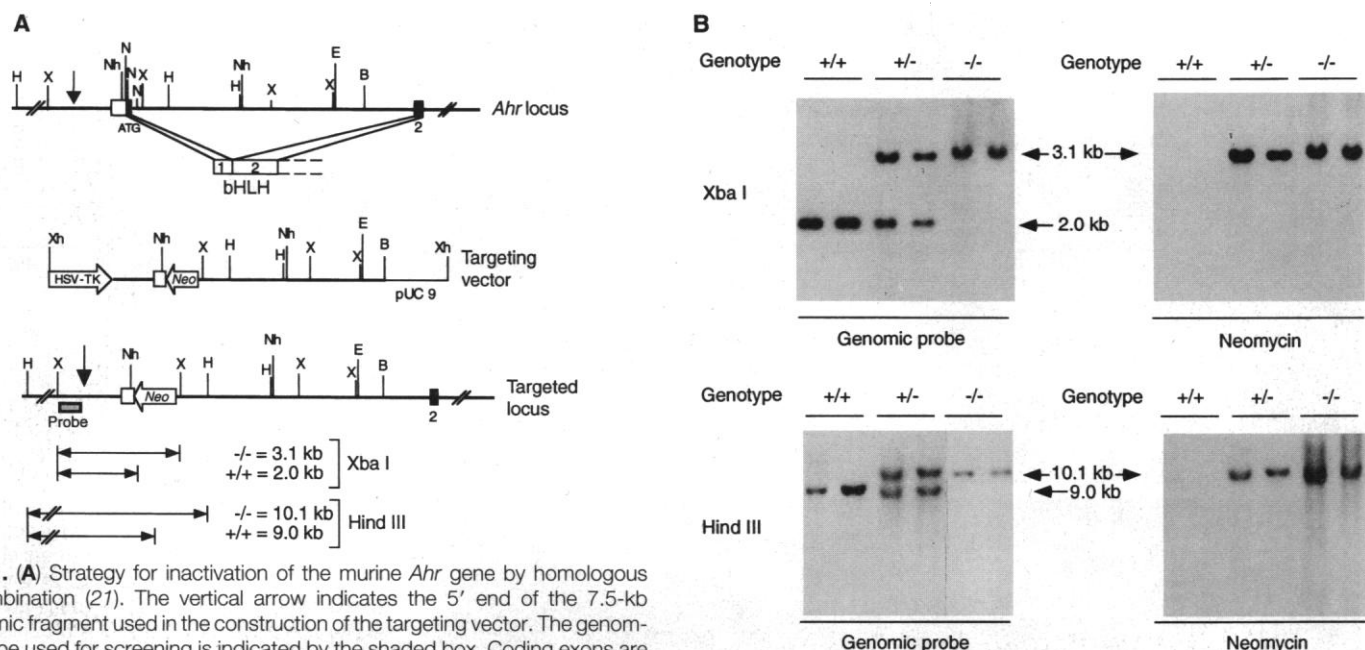


Fig. 1. (A) Strategy for inactivation of the murine *Ahr* gene by homologous recombination (21). The vertical arrow indicates the 5' end of the 7.5-kb genomic fragment used in the construction of the targeting vector. The genomic probe used for screening is indicated by the shaded box. Coding exons are indicated by black boxes. The 5' untranslated region of the gene is represented by an open box. bHLH, the bHLH domain of the AHR. Restriction endonucleases: B, Bam HI; E, Eco RI; H, Hind III; N, Nar I; Nh, Nhe I; X, Xba I; and Xh, Xho I. (B) Southern blot analysis of mouse tail genomic DNA (22). Genomic DNA was isolated from tails and digested with either Xba I or Hind III. Xba I generated 2.0- and 3.1-kb bands for the wild-type (+) and targeted (-) alleles, respectively; Hind III yielded 9.0- and 10.1-kb bands for the wild-type and targeted alleles, respectively. The fidelity of the recombination event was confirmed by hybridization with the neomycin cassette as a probe; only the bands corresponding to the targeted allele hybridize with the probe. Two different animals for each genotype are shown. (C) Northern blot analysis of transcripts that encode major AHR-regulated phase I and phase II enzymes that participate in the hepatic detoxification process. Six-week-old littermates were treated with solvent or TCDD (23) and total liver RNA was then subjected to Northern analysis (24). For comparative purposes, results corresponding to the same exposure time for the different genes are shown; longer exposures allow the detection and quantification of the constitutive amounts of *Cyp1a2* and *Ugt1*06* mRNAs in the liver of *Ahr*^{-/-} mice. Actin mRNA was analyzed to monitor the integrity of RNA.

birth; although the precise cause of death could not be determined, necropsy analysis revealed lymphocyte infiltration of various organs, particularly the gut, urinary tract, and lung. Surviving *Ahr*^{-/-} mice had a slower growth rate within the first 2 to 4 weeks of age as compared with *Ahr*^{+/+} or *Ahr*^{+/-} littermates, but they usually reached adulthood and were fertile. The animals were housed in a germfree facility and were fed with sterilized Purina rodent chow. Drinking water was filtered and chlorinated to 8 to 10 parts per million.

The AHR is required for dioxin inducibility of such murine genes as *Cyp1a1*, *Cyp1a2*, and *Ugt1*06* and interacts with aromatic hydrocarbon-responsive elements (AhREs) upstream of each gene (6, 13, 17).

Both *Cyp1a2* and *Ugt1*06* are constitutively expressed in liver, whereas *Cyp1a1* is expressed in this organ only in the presence of inducer (18). To determine the role of the AHR in the regulation of these genes, we studied their constitutive and dioxin-induced expression by Northern (RNA) blot analysis (Fig. 1C). Whereas *Ahr*^{+/+} animals exhibited maximal induction of *Cyp1a1* by dioxin, this effect was abolished in *Ahr*^{-/-} mice, demonstrating that a functional AHR is required for induction in liver. Similar results were obtained in lung and kidney. The abundance of *Cyp1a2* and *Ugt1*06* mRNAs was also increased in the liver of *Ahr*^{+/+} animals after dioxin treatment (8- to 10-fold and 2- to 3-fold, respectively), but induction was not observed in

either liver or kidney of *Ahr*^{-/-} mice. The absence of the AHR was also associated with decreases of $90 \pm 5\%$ and $85 \pm 5\%$ (means \pm SD, $n = 6$), respectively, in the constitutive amounts of *Cyp1a2* and *Ugt1*06* transcripts in liver. Thus, in the absence of exogenous ligand, the AHR controls basal gene expression; these data suggest either that trans-activation of some genes occurs in the absence of endogenous ligand or that an endogenous ligand occupies the binding site on the AHR, allowing its interaction with certain AhREs.

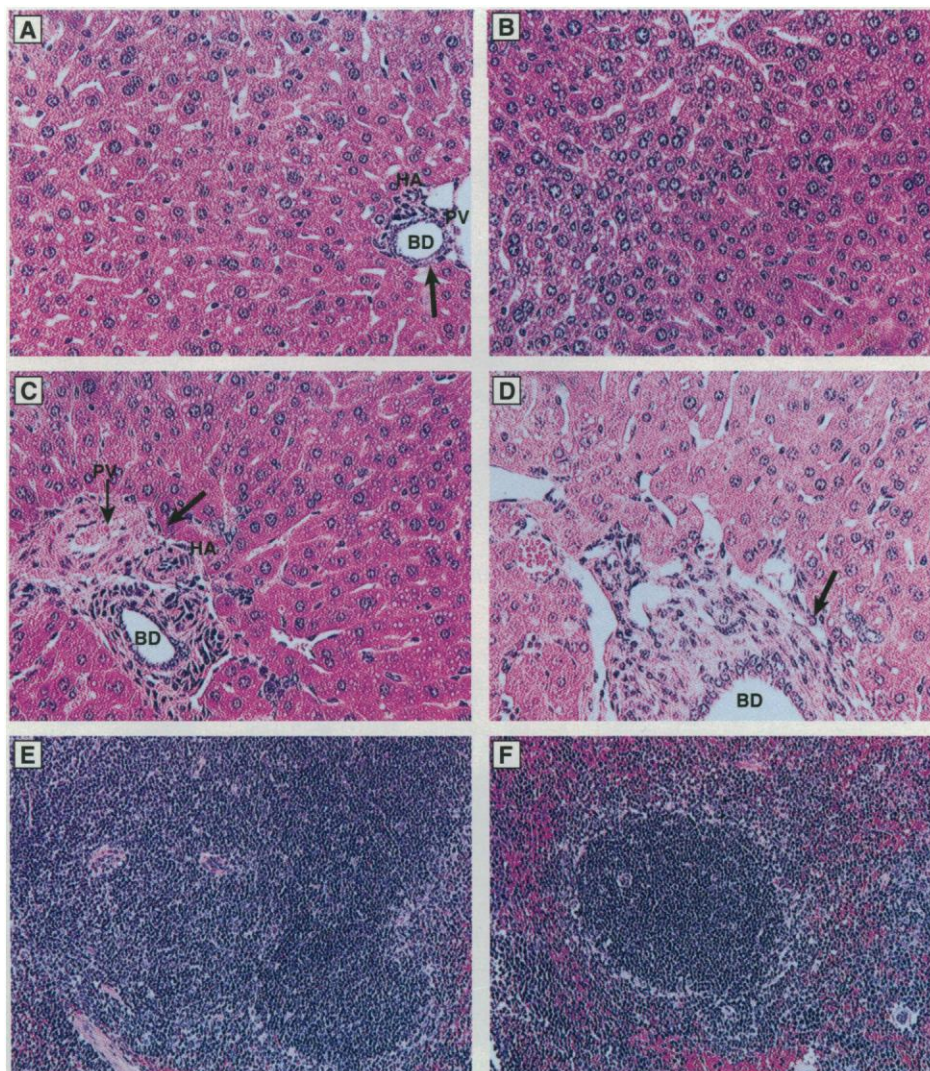


Fig. 2. Histological analysis of hepatic and splenic tissues from 4-week-old *Ahr*^{-/-} and *Ahr*^{+/+} littermates. (A) Normal liver parenchyma and normal portal tract from an *Ahr*^{+/+} mouse. HA, hepatic artery; PV, portal vein; and BD, bile duct. (B) Hypercellularity in an *Ahr*^{-/-} mouse liver; small hepatocytes with little cytoplasm are concentrated toward the centrilobular area of the liver. (C and D) Development of fibrosis (moderate at this stage) in *Ahr*^{-/-} mice. The connective tissue surrounding the portal tract is indicated by a thick arrow. (E and F) Histology of spleen from *Ahr*^{+/+} (E) and *Ahr*^{-/-} (F) mice. Organs were removed, weighed, and fixed in formalin solution (10% formaldehyde in phosphate-buffered saline); sections (5 μ m) were prepared and stained with hematoxylin-eosin. Magnification: $\times 180$ (A to D), $\times 13$ (E and F).

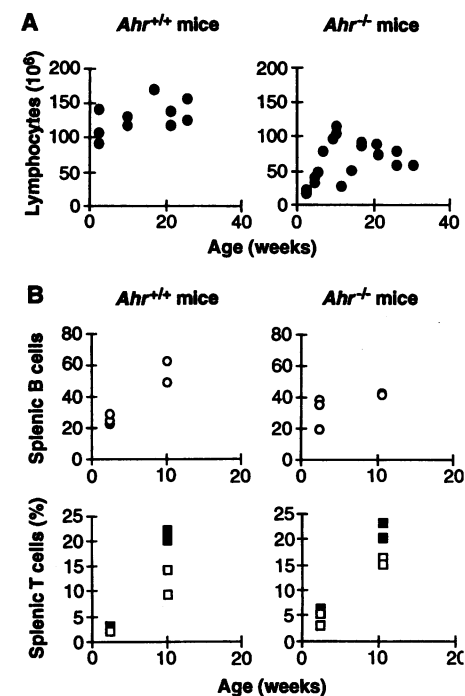


Fig. 3. Quantitative analyses of number and cell surface phenotype of splenic lymphocytes in *Ahr*^{+/+} and *Ahr*^{-/-} mice. (A) Number of splenic lymphocytes recovered from *Ahr*^{+/+} and *Ahr*^{-/-} mice at various ages. Cell counts reflect the number of trypan blue-excluding, nucleated cells observed microscopically; each data point represents the total number of such cells recovered from a single mouse of the indicated genotype. (B) Proportion of splenic B cells and T cells obtained from wild-type and mutant mice at 2 and 10 weeks after birth. B cells were identified by the expression of CD45R(B220) (○) and T cells by the expression of CD4 (■) and CD8 (□). Results from three mice at 2 weeks and two mice at 10 weeks of age are shown. All 2-week-old mice were littermates, as were the 10-week-old animals. Each data point represents the proportion of cells stained by fluorescein isothiocyanate- or phycoerythrin-labeled monoclonal antibodies specific for the indicated cell surface antigen. All staining reagents were obtained from Pharmingen (San Diego, California). Data were collected and analyzed on a FACScan with LYSYS II software (Becton Dickinson, Palo Alto, California). Red blood cells were excluded by forward scatter. Dead cells were excluded by propidium iodide staining. In some graphs, data points overlap and are therefore not fully visible.

The AHR is expressed in many tissues in both mice (9) and humans (19). To investigate the systemic effects of AHR deficiency, we compared the major internal organs of *Ahr*^{-/-} and *Ahr*^{+/+} mice. Lung, kidney, brain, heart, bone marrow, muscle, adrenal gland, thyroid, and intestine showed no obvious histological abnormalities in *Ahr*^{-/-} animals. In contrast, liver tissue from *Ahr*^{-/-} mice differed both quantitatively and qualitatively from that isolated from *Ahr*^{+/+} animals. Livers from 4-week-old *Ahr*^{-/-} mice constituted $2.9 \pm 0.3\%$ ($n = 15$) of body mass, compared to $6.1 \pm 0.4\%$ ($n = 15$) in *Ahr*^{+/+} or *Ahr*^{+/-} animals. Histological examination (Fig. 2, A to D) revealed that the general structure of the hepatic lobules was normal in *Ahr*^{-/-} mice. However, these animals developed pronounced fibrosis in the portal tract; spontaneous liver fibrosis in mice is extremely rare and normally can be induced only by several hepatotoxins (20). This phenomenon was apparent already at 3 weeks of age in *Ahr*^{-/-} mice. Some *Ahr*^{-/-} mice also showed mild to moderate inflammatory changes in the bile ducts (cholangitis). Eosinophilia resembling that seen after treatment of mice with certain foreign chemicals was consistently apparent in periportal hepatocytes. *Ahr*^{-/-} mice also showed centrilobular hypercellularity and glycogen de-

pletion. Nevertheless, no instance of sclerosing cholangitis was severe enough to be lethal in the absence of chronic treatment with dioxin. These results suggest that the histological defect might impair liver function in *Ahr*^{-/-} mice, possibly contributing to their lower rate of growth at early ages (2 to 4 weeks). The AHR may exert a protective effect against endogenous or dietary chemicals during development.

To evaluate the effects of AHR deficiency on the development and maintenance of the immune system, we compared the cellular composition and cell surface phenotype of thymic and splenic cells obtained from *Ahr*^{+/+} and *Ahr*^{-/-} mice. Histological analyses of spleen demonstrated that 4-week-old *Ahr*^{+/+} mice developed normal splenic architecture (Fig. 2E), whereas age-matched *Ahr*^{-/-} mice had smaller, although structurally normal, periarterial lymphatic sheaths (Fig. 2F). A quantitative comparison of splenic lymphocyte numbers between *Ahr*^{+/+} and *Ahr*^{-/-} mice indicated that this difference varied with the age of the animal (Fig. 3A). In particular, *Ahr*^{-/-} mice at 2 to 3 weeks of age contained 75 to 85% fewer lymphocytes than did *Ahr*^{+/+} littermates. As *Ahr*^{-/-} mice aged, the number of splenic lymphocytes increased to approximately normal numbers by 10 to 12 weeks after birth. The oldest *Ahr*^{-/-} mice tested (25 to 32 weeks) showed a decrease in lymphocytes to ~50% of the number in *Ahr*^{+/+} controls. Similar analyses also indicated that peripheral lymph nodes from *Ahr*^{-/-} mice contained fewer lymphocytes than those from *Ahr*^{+/+} mice.

The difference in the absolute numbers of peripheral lymphocytes between young *Ahr*^{+/+} and *Ahr*^{-/-} mice suggested that mutant mice may either lack a specific lymphoid subpopulation or, alternatively, display a systemic defect in the ability of lymphocytes to reside in the periphery. To distinguish between these possibilities, we assessed the expression of T cell- and B cell-specific surface markers on splenic lymphocytes obtained from wild-type and mutant mice at 2 and 10 weeks of age (Fig. 3B). Comparison of age-matched *Ahr*^{+/+} and *Ahr*^{-/-} mice indicated that they contained similar proportions of B cells as determined by expression of CD45R(B220). Similarly, the proportions of T cells, as assessed by CD4 and CD8, were also similar between wild-type and mutant animals of the same ages. Analyses of lymph node populations indicated that, although fewer cells were present, the cell surface phenotype and the ratio between T and B cells appeared normal. Thus, the AHR deficiency results in an apparent delay in the seeding of peripheral T and B lymphocytes.

To determine whether this delayed development was restricted to the peripheral

immune system or whether other lymphoid organs were also affected by the absence of AHR, we assessed the cellular composition and surface phenotype of cells within the thymus of *Ahr*^{+/+} and *Ahr*^{-/-} mice. Neither the absolute number (Fig. 4A) nor the proportion of single-positive (CD4⁺CD8⁻ or CD4⁻CD8⁺) or double-positive (CD4⁺CD8⁺) thymocytes (Fig. 4B) differed between *Ahr*^{-/-} and age-matched *Ahr*^{+/+} mice. The expression of CD3 and the $\alpha\beta$ T cell receptor also appeared normal on *Ahr*^{-/-} thymocytes, further suggesting that AHR deficiency does not affect the development of normal thymic subpopulations.

The mechanisms by which AHR deficiency delays the appearance of peripheral lymphocytes and subsequently decreases their number in mutant animals remain unclear. However, AHR deficiency may affect the normal process of positive selection in the thymus or emigration from the bone marrow, thereby limiting the number of lymphocytes entering the periphery. Such a scenario would allow for the generation of apparently normal numbers of progenitor B and T cells, but only a small fraction would successfully emigrate to the periphery. Alternatively, AHR deficiency may not affect the production of competent lymphocytes but rather may interfere with their ability to home efficiently to the appropriate peripheral lymphoid organ; those cells displaying inappropriate homing specificities would be subject to elimination. Finally, AHR deficiency may simply shorten the normal life-span of peripheral lymphocytes. In young animals, which generate large numbers of immune cells, a shortened half-life may only delay the accumulation of peripheral lymphocytes. In contrast, older mice, in which production of newly emerging lymphocytes has diminished, would likely experience a decrease in the absolute number of peripheral lymphocytes as a result of a shortened lymphocyte life-span.

Ahr^{-/-} mice should prove useful for studies of carcinogenesis and chemical risk assessment with regard to various important highly toxic environmental pollutants. The effects of these chemicals on the liver and the immune system without the mediation of the AHR will help clarify the genotoxic and nongenotoxic pathways for tumor initiation, promotion, and progression as well as for mutagenesis and toxicity. In addition, this mouse line will help delineate the role of the AHR in normal development of the liver and the immune system.

REFERENCES AND NOTES

1. H. I. Swanson and C. A. Bradfield, *Pharmacogenetics* 3, 213 (1993).
2. E. C. Hoffman *et al.*, *Science* 252, 954 (1991); H. Li, L. Dong, J. P. Whitlock Jr., *J. Biol. Chem.* 269,

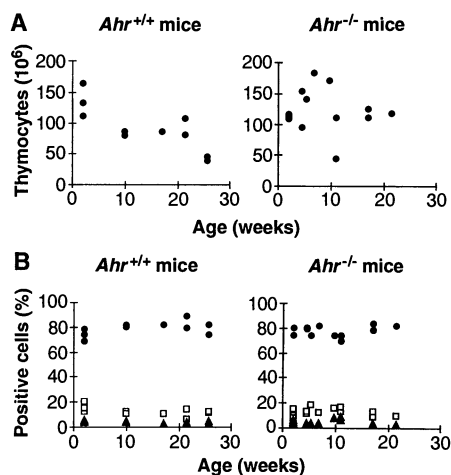


Fig. 4. Quantitative analyses of number and cell surface phenotype of thymocytes from *Ahr*^{+/+} and *Ahr*^{-/-} mice. **(A)** Total number of thymocytes recovered from mice of the indicated ages. Cell counting was performed as described in the legend to Fig. 3. **(B)** The cell surface phenotype of thymocytes was determined with phycoerythrin-labeled monoclonal antibodies to CD4 and fluorescein isothiocyanate-labeled monoclonal antibodies to CD8 (25). The double-positive (CD4⁺CD8⁺) (●) and single-positive [CD4⁺CD8⁻ (□) and CD4⁻CD8⁺ (▲)] subpopulations were identified by two-color flow cytometry as described in Fig. 3. Each data point represents the proportion of thymocytes in a single thymus expressing the indicated antigen.

- 28098 (1994); M. L. Whitelaw, J.-A. Gustafsson, L. Poellinger, *Mol. Cell. Biol.* **14**, 8343 (1994).
3. A. B. Okey, D. S. Riddick, P. A. Harper, *Trends Pharmacol. Sci.* **15**, 226 (1994).
 4. G. W. Lucier, C. J. Portier, M. A. Gallo, *Environ. Health Perspect.* **101**, 36 (1993); M. J. DeVito, X. Ma, J. G. Babish, M. Menache, L. Birnbaum, *Toxicol. Appl. Pharmacol.* **124**, 82 (1994); H. Huoskonen, M. Unkila, R. Pohjanvirta, J. Tuomisto, *ibid.*, p. 174; P. A. Bertazzi *et al.*, *Epidemiology* **4**, 398 (1993); L. S. Birnbaum, *Environ. Health Perspect.* **102**, 676 (1994).
 5. D. J. McConkey, P. Hartzell, S. K. Duddy, H. Hakansson, S. Orrenius, *Science* **242**, 256 (1988).
 6. D. W. Nebert, *CRC Crit. Rev. Toxicol.* **20**, 153 (1989).
 7. _____, D. D. Peterson, A. Puga, *Pharmacogenetics* **1**, 68 (1991).
 8. W. Li, S. Donat, O. Dohr, K. Unfried, J. Abel, *Arch. Biochem. Biophys.* **315**, 279 (1994).
 9. K. M. Dolwick *et al.*, *Mol. Pharmacol.* **44**, 911 (1993).
 10. S. Kimura, F. J. Gonzalez, D. W. Nebert, *Mol. Cell. Biol.* **6**, 1471 (1986).
 11. F. J. Gonzalez and D. W. Nebert, *Nucleic Acids Res.* **13**, 7269 (1985).
 12. U. Savas *et al.*, *J. Biol. Chem.* **269**, 14905 (1994); T. R. Sutter *et al.*, *ibid.*, p. 13092; Z. Shen *et al.*, *DNA Cell Biol.* **13**, 763 (1994).
 13. T. R. Sutter, K. Guzman, K. M. Dold, W. F. Greenlee, *Science* **254**, 415 (1991); A. Puga, D. W. Nebert, F. Carrier, *DNA Cell Biol.* **11**, 269 (1992).
 14. B. D. Abbott, G. H. Perdew, L. S. Birnbaum, *Toxicol. Appl. Pharmacol.* **126**, 16 (1994); D. W. Nebert, *Biochem. Pharmacol.* **47**, 25 (1994).
 15. M. Capecchi, *Science* **244**, 1288 (1989).
 16. S. L. Mansour *et al.*, *Nature* **336**, 348 (1988).
 17. F. J. Gonzalez, *Pharmacol. Rev.* **40**, 243 (1989); R. W. Robertson, L. Zhang, D. S. Pasco, J. B. Fagan, *Nucleic Acids Res.* **22**, 1741 (1994); J. O. Miners and P. I. Mackenzie, *Pharmacol. Ther.* **51**, 347 (1991).
 18. F. J. Gonzalez and D. W. Nebert, *Trends Genet.* **6**, 182 (1990).
 19. S. Hayashi *et al.*, *Carcinogenesis* **15**, 801 (1994).
 20. A. Poland and J. C. Knutson, *Annu. Rev. Pharmacol. Toxicol.* **22**, 517 (1982).
 21. To inactivate the *Ahr* gene in ES cells, we isolated a genomic clone from a 129/SV mouse library (Stratagene) with a 96-nucleotide oligomer complementary to the 5' coding region of the murine AHR complementary DNA [nucleotides 978 to 1073 in M. Ema *et al.*, *Biochem. Biophys. Res. Commun.* **184**, 246 (1992)]. A 7.5-kb fragment containing exon 1 from this genomic clone was digested with Sal I (phage vector cloning site) and Bam HI, and cloned into the vector pMC-TK (negative selection marker conferred by the HSV-TK cassette). To generate the replacement targeting construct, we deleted the coding exon 1 by digestion with Nar I and insertion of a modified *neo*-poly(A) cassette (positive selection marker that confers resistance to G418) with compatible Cla I ends. The final construct in pUC9 was linearized at a unique Xho I site and introduced by electroporation into 1×10^7 ES cells with a Bio-Rad Gene Pulser (250 V, 250 μ F). Electroporated ES cells were plated onto a monolayer of γ -irradiated, neomycin-resistant mouse primary fibroblasts and the cells were grown in the presence of leukemia inhibitor factor (1000 U/ml) (Gibco BRL). Selection was performed for 7 to 8 days with G418 (350 μ g/ml) and 5 μ M ganciclovir. Surviving clones were isolated and analyzed for the homologous recombination event.
 22. Genomic DNA was digested with Xba I or Hind III and subjected to electrophoresis on 0.7 and 0.45% agarose gels, respectively. The gels were blotted under alkaline conditions with Gene Screen Plus nylon membranes (DuPont), which were then hybridized at 42°C in 10% dextran sulfate—50% formamide solution with random primer-labeled genomic DNA probe or neomycin cassette at a radioactive concentration of 1.5×10^6 cpm/ml. The membranes were washed at 65°C for 30 min in $2 \times$ standard saline citrate (SSC) containing 0.5% SDS and then for 15 min in $1 \times$ SSC containing 0.5% SDS.
 23. Animals were administered a single intraperitoneal injection (25 μ l) of TCDD (Accu-Standard) dissolved in 1,4-dioxane (Baxter) at a dose of 40 μ g per kilo-

gram of body mass. Control animals were injected with the same volume of pure solvent. Mice were killed by carbon monoxide asphyxiation 20 hours after injection. The organs were removed rapidly, weighed, and stored in liquid nitrogen until use. TCDD was of the highest purity commercially available (>99%) and 1,4-dioxane was of high performance liquid chromatography quality.

24. Total liver RNA was isolated from the frozen tissues according to the guanidinium-thiocyanate method [P. Chomczynski and N. Sacchi, *Anal. Biochem.* **162**, 156 (1987)] and 15 μ g were applied to 1% agarose-formaldehyde gels. The gels were blotted onto Gene Screen Plus nylon membranes, which were then hybridized at 42°C in 10% dextran sulfate—50% formamide solution containing the appropriate murine complementary DNA probes. The membranes were washed at 65°C for 30 min in $2 \times$ SSC containing

0.5% SDS and then for 20 min in $0.5 \times$ SSC containing 0.5% SDS. Quantitation of the amounts of mRNA was performed by exposing blots to Phosphor Screens (Eastman-Kodak) for 24 hours. The screens were then analyzed with a Phosphorimager (Molecular Dynamics) and the signals were quantified by volume integration with software provided by the manufacturer.

25. D. M. Hilbert, K. L. Holmes, A. O. Anderson, S. Rudikoff, *Eur. J. Immunol.* **23**, 2412 (1993).
26. We thank U. Hochgeschwender for the J1 cells, which were originally provided by R. Jaenisch, and for technical support; D. Accili for helpful suggestions; and G. Miller, E. Lee, and H. Westphal for technical assistance. Supported in part by NIH grants R01 ES06811 and P30 ES06096 to D.W.N.

14 December 1994; accepted 24 February 1995

Inhibition of Proteasome Activities and Subunit-Specific Amino-Terminal Threonine Modification by Lactacystin

Gabriel Fenteany, Robert F. Standaert, William S. Lane, Soongyu Choi, E. J. Corey, Stuart L. Schreiber*

Lactacystin is a *Streptomyces* metabolite that inhibits cell cycle progression and induces neurite outgrowth in a murine neuroblastoma cell line. Tritium-labeled lactacystin was used to identify the 20S proteasome as its specific cellular target. Three distinct peptidase activities of this enzyme complex (trypsin-like, chymotrypsin-like, and peptidylglutamyl-peptide hydrolyzing activities) were inhibited by lactacystin, the first two irreversibly and all at different rates. None of five other proteases were inhibited, and the ability of lactacystin analogs to inhibit cell cycle progression and induce neurite outgrowth correlated with their ability to inhibit the proteasome. Lactacystin appears to modify covalently the highly conserved amino-terminal threonine of the mammalian proteasome subunit X (also called MB1), a close homolog of the LMP7 proteasome subunit encoded by the major histocompatibility complex. This threonine residue may therefore have a catalytic role, and subunit X/MB1 may be a core component of an amino-terminal-threonine protease activity of the proteasome.

Lactacystin (compound **2** in Fig. 1) was discovered on the basis of its ability to induce neurite outgrowth in the murine neuroblastoma cell line Neuro-2a (1). Lactacystin also inhibits proliferation of other cell types, suggesting that its target is not exclusive to Neuro-2a cells (2). To understand the cellular effects of lactacystin, we tested a series of analogs and found that a synthetic β -lactone (compound **1** in Fig. 1) related to lactacystin showed similar biological activity, whereas the corresponding acid, formally the product of hydrolysis of the lactacystin thioester or the β -lactone, did not (2). These and other data suggested that an electrophilic carbonyl at C4 was essential for the biological activity of lacta-

cystin, and thus that its target might be an enzyme containing a catalytic nucleophile, such as a protease or a lipase (2). The C4 carbonyls of both the thioester and the β -lactone are reactive electrophiles, whereas the carboxylate of the dihydroxy acid is essentially inert to nucleophilic attack.

To purify and identify the target, we synthesized [3 H]lactacystin and the [3 H] β -lactone at a specific activity of 3.4 Ci/mmol (Fig. 1). Incubation of crude extracts from Neuro-2a cells or bovine brain with [3 H]lactacystin (or [3 H] β -lactone), followed by SDS-polyacrylamide gel electrophoresis (SDS-PAGE) and fluorography, revealed the presence of an intensely labeled protein band of ~24 kD (Fig. 2) and a weakly labeled band at ~32 kD. The latter is not evident in Fig. 2 and appeared only with prolonged exposure times, but the 24-kD band was visibly radiolabeled even after a 5-min treatment with 1 μ M [3 H] β -lactone or [3 H]lactacystin (3). Similar results were obtained with extracts from *Saccharomyces cerevisiae* and bovine liver and thymus. La-

G. Fenteany, R. F. Standaert, S. L. Schreiber, Howard Hughes Medical Institute, Departments of Chemistry and Molecular and Cellular Biology, Harvard University, Cambridge, MA 02138, USA.
W. S. Lane, Harvard Microchemistry Facility, Harvard University, Cambridge, MA 02138, USA.
S. Choi and E. J. Corey, Department of Chemistry, Harvard University, Cambridge, MA 02138, USA.

*To whom correspondence should be addressed.